2022

Study the C-V behavior of cesium-lead halides perovskite solar cells under various simulation parameters

Zahraa Ismail
zahraa.ismail@bue.edu.eg

Eman Farouk Sawires
Helwan University, eman_sedhom@h-eng.helwan.edu.eg

Fathy Zaki Amer
Helwan University, Fathy_amer@h-eng.helwan.edu.eg

Sameh O. Abdellatif Dr
The British University in Egypt

Study the C-V behavior of cesium-lead halides perovskite solar cells under various simulation parameters

Zahraa S. Ismail
Electrical Engineering Department
Faculty of Engineering and FabLab in the Center for Emerging Learning Technology (CELT)
The British University in Egypt
Cairo, Egypt
Zahraa.ismail@bue.edu.eg

Eman F. Sawires
Electronics and Communications Engineering Department
Faculty of Engineering, Helwan University
Cairo, Egypt
eman_sedhom@h-eng.helwan.edu.eg

Fathy Z. Amer
Electronics and Communications Engineering Department
Faculty of Engineering, Helwan University
Cairo, Egypt
Fathy_amer@h-eng.helwan.edu.eg

Sameh O. Abdellatif
Electrical Engineering Department
Faculty of Engineering and FabLab in the center for Emerging Learning Technology(CELT), The British University in Egypt(BUE)
Cairo, Egypt
Sameh.osama@bue.edu.eg

2022 International Conference on Green Energy, Computing and Sustainable Technology (GECOST) | 978-1-6654-8663-7/22/$31.00 ©2022 IEEE | DOI: 10.1109/GECOST55694.2022.10010474

***Abstract*— Capacitance response of perovskite solar cells (PSCs) can be oppressed to deduce underlying physical mechanisms, both in the materials at external interfaces and in bulk materials. Accordingly, this paper investigates the Capacitance-Voltage (C-V) characteristic curves of cesium lead halides ($CsPbX_3$: X = I, Br, or Cl) used as an active layer in PSCs. The SCAPS-1D simulator harnessed the actual device ($CsPbX_3$: X = I Br, or Cl) with material parameters from previous experimental work. Three main simulation parameters were investigated: the thickness of the active layer, the doping, and the defects impacts.**

Keywords*—Perovskite Solar cell, $CsPbX_3$, SCAPS-1D, Power Conversion Efficiency, C-V characteristics.

I. INTRODUCTION

Perovskite solar cells (PSCs) are a class of novel third-generation photovoltaic (PV) solar cells. PSCs can replace conventional solar cells due to their significant absorption coefficient, long carrier diffusion length, small exciton binding energy, lower cost, ease of fabrication, and high device performance. They can be fabricated as multi-junction (tandem) cell and single junction architectures. The optoelectronic, mechanical, and physical properties of perovskites are appropriate for the PV application [1-8]. A typical PSC employed organic-inorganic halide material as active/absorber material. The power conversion efficiency (PCE) of PSCs has increased progressively over the last ten years, from 3.8% in 2009 to 25.5% in 2022 [9].

Alternatively, the perovskite absorber layer is thermally and chemically unstable due to the essential instability of the organic cation present in it [10-12]. Thus, reducing the shelf life of the perovskite compound and leading to the limitation of its widespread commercialization. Recent studies state that the stability of PSCs can be improved by substituting the hybrid organic-inorganic absorber layer with an inorganic halide perovskite layer without compromising the device performance [6, 8, 11-13]. Lately, Cesium (Cs^+) has replaced the volatile organic components due to their intrinsic inorganic stability with no crystal lattice distortion, chemical degradation, and superior PV performance [11-13]. Inorganic cesium lead halide ($CsPbX_3$, X = I, Br, and Cl) perovskites have been reported as early as 1893, have good thermal stability, and are considered among the most promising materials suitable for the development of inorganic PSCs [8, 11, 13]. $CsPbI_3$ with the cubic phase exhibits the most suitable bandgap of 1.73 eV for PV applications with excellent potential for high-efficiency inorganic PSCs [8, 12, 13]. However, $CsPbI_3$ still has exceptional stability under moist circumstances. Thus, vital contributions are still essential for achieving long-term stability. $CsPbBr_3$ holds excellent moisture stability with a high bandgap of 2.3 eV. It has been used to fabricate PSCs with high PCEs up to 10.5%. $CsPbCl_3$ shows the lowest efficiency with the greatest bandgap of 3 eV among all cesium lead halides [6, 8, 11-13].

This work aims to provide a deep understanding of the effect of doping density, thickness, and defect density of the absorber layer on the PSC performance for enhancing and optimizing the performance of PSCs. The simulation and modeling of PSC provide a deep understanding of the physics of the device and elucidate the inter-relationship between the performance of the device and the material properties of each layer.

Discovering and analyzing the PV performance of Cesium lead halides through simulation studies allow the research community to recognize the pros and cons of using them as absorber layers in PSCs. The results presented in this work deliver cooperative guidance for fabricating all-inorganic PSCs with high efficiency and good stability.

II. C-V SIMULATION MODELS

SCAPS is used for the present study on perovskite inorganic halides ($CsPbI_3$, $CsPbBr_3$, and $CsPbCl_3$) and to understand the performance of PSC via computational investigations [2, 3, 14-16].

The stack of simulated PSC consists of several layers: Ag/NiO/Perovskite layer/TiO_2/FTO, as shown in Figure 1. The default generation model of SCAPS is used and the solar illumination for all simulation is considered to be AM 1.5G (1000 Wm^{-2}) at 300 K temperature. No Auger recombination

and radiative band-to-band recombination are considered. PSC used in the simulation is an n-i-p structure laid between the p-type NiO as an hole transport layer (HTL) with a total defect density N_t of 1 x 10^{15} cm^{-3}, which transports holes in PSC and performs as an electron blocking layer (EBL) for reducing charge recombination, and (compact and mesoporous) n-type semiconductor Titanium Oxide (TiO_2) as electron transport layer (ETL) with total defect density N_t of 1 x 10^{15} cm^{-3}. They have deposited on the top of Fluorine doped Tin Oxide (FTO) substrate, the transparent conductive oxide (TCO) that serves as an s window layer, forming the photo-anode. The compact layer of TiO_2 was used to prevent electrode shorting. Au (Gold) is the contact layer with a work function of 5.1 eV. The absorber layer ($CsPbI_3$, or $CsPbBr_3$, or $CsPbCl_3$) or called the active layer, which is the heart of the solar cell device. The bandgaps of $CsPbI_3$, $CsPbBr_3$, and $CsPbCl_3$ are 1.73 eV, 2.3 eV, 3 eV, respectively that make them favorable for PV applications. The three different absorber layers are $CsPbI_3$, $CsPbBr_3$, and $CsPbCl_3$, which are n-type, p-type material, and p-type, respectively, as proved in several works [2, 3, 14-16]. The thermal velocity of holes and electrons for all various layers is set as 1 x 10^7 cm/s. The valence band and conduction band offsets among absorber/HTL and buffer/absorber layers are set to be 0.0 eV by adjusting the electron affinity of the buffer and HTL, respectively. The absorption coefficient (α) is used as the default value is 10^6 m^{-1}. The numerous simulation parameters adopted from different experimental and theoretical studies are shown in Table 1.

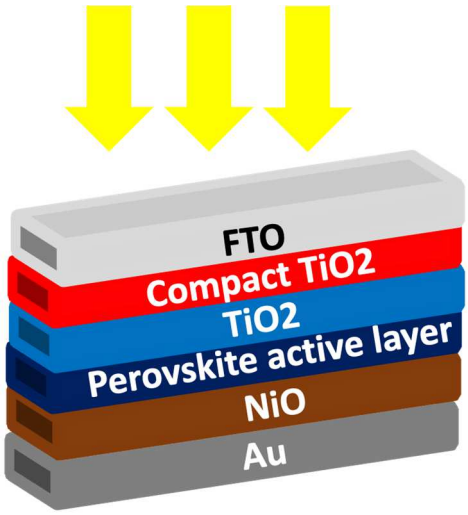

Figure 1. The schematic diagram for perovskite solar cell simulated using SCAPS.

II. SIMULATION RESULTS AND DISCUSSIONS

A. C-V curve characteristic of the simulated device

Capacitance-Voltage (C-V) characteristic curve is beneficial and helpful in attaining a better insight of capacitance on the PSC, which depends on the applied voltage. The association was done by scanning a dc voltage from 0 to 3 V at 1 M Hz. The extension of the depletion region starts at the perovskite layer/Au interface as the voltage bias increases from 0 V, then it goes through the perovskite layer and finally to TiO_2. Subsequently, more charges will be accumulated at the interfaces (perovskite/TiO_2 and NiO/perovskite) by increasing the applied voltage bias that induces higher capacitance until a specific voltage (V_{oc}) as 1.3 V, 2.257 V, and 1.6 V for $CsPbI_3$, $CsPbBr_3$, and $CsPbCl_3$, respectively. As shown in Figure 2, $CsPbI_3$-based PSC has the least accumulated capacitance on both interfaces as it has the most nominal peak voltage compared to $CsPbBr_3$-based PSC and $CsPbCl_3$-based PSC. $CsPbBr_3$-based PSC has the highest built-in voltage (V_{bi}) among other PSCs, with the maximum accumulation capacitance at the interfaces.

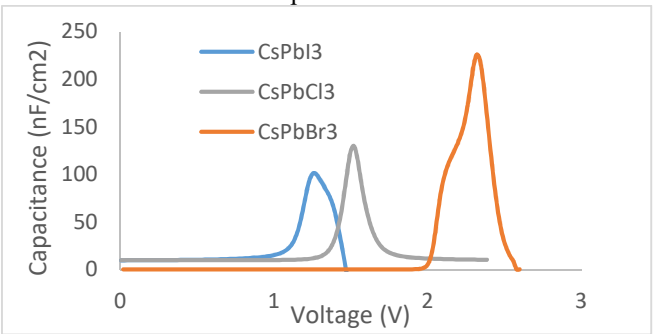

Figure 2. C-V curves for the three cesium lead halides discussed in this paper.

B. Thickness impact on the C-V characteristics

As the active layer thickness increases from 100 nm to 2µm, the sandwiched layer absorbs more incident photons from the light to generate the electron-hole pairs. Therefore, more charges are accumulated at the NiO/perovskite and perovskite/TiO_2 interfaces due to the weakening of V_{bi} that leads to an increase in the accumulated capacitance at interfaces until reaching peak voltage (V_{peak}) for the three absorber layers. Afterwards, the charge carriers start to recombine when V_{bi} is totally dimensioned by the further increase beyond V_{peak}. In addition, there is a little decrement in the value of V_{bi} by increasing the thickness.The C-V curve variation concerning the thickness of the absorber layer has been drawn as shown in curves (a) $CsPbI_3$, (b) $CsPbBr_3$, and (c) $CsPbCl_3$ in figure 3.

C. Doping impact on the C-V characteristics

As the doping density increases till the defect density as 1x10^{15} cm^{-3}, 1x10^{19} cm^{-3} and 1x10^{15} cm^{-3} for $CsPbI_3$, $CsPbBr_3$, and $CsPbCl_3$, respectively, the C-V curve remains constant. This means that the doping density less than the defect density has no effect on the behavior of the C-V curve for the three absorber layers as the generation rate of photogenerated carriers does not alter with dopant densities under the incident of the same photon number. The fermi energy level of the charge decreases with increasing the dopant concentration. As the doping density increases beyond the defect density, the electric field and V_{bi} increases as shown in Figure 4(a) for $CsPbI_3$, (b) for $CsPbBr_3$, and (c)$CsPbCl_3$. Charge seperation take place rapidly with an increase in the value of electric field charge carriers, leading to improved device efficiency and hence increase in V_{oc}. Therefore, the C-V curves are shifted with higher V_{bi} and V_{oc} as well as higher accumulated capacitance on both interfaces. Moreover, capacitance value increase with less peak voltages as shown in Figure 4(a) for $CsPbI_3$, (b) for $CsPbBr_3$, and (c)$CsPbCl_3$.

D. Defects impact on the C-V characteristics

The variation of defect density may play a vital role in improving the performance of the low-quality absorbing layer that leads to the maximum recombination rate of the carrier that affects the device output, see figure 5.

Table I: Simulation parameters of PSCs devices.

Parameters	TCO	ETL (TiO_2)	Absorber ($CsPbI_3$)	Absorber ($CsPbBr_3$)	Absorber ($CsPbCl_3$)	HTL(NiO)
Thickness (μm)	0.300 – 3.50	0.030	0.500	0.500	0.500	0.245
Band gap energy E_g (eV)	3.5	3.2	1.73	2.32	3.06	3.6
Electron affinity χ (eV)	4	4.26	3.95	3.6	3.3	1.8
Relative permittivity e_r	9	9	6	6.5	5.355	11.75
Effective conduction band density N_c (cm^{-3})	2.2×10^{18}	1×10^{18}	1.1×10^{20}	4.94×10^{17}	1×10^{18}	2×10^{18}
Effective valance band density N_v (cm^{-3})	1.8×10^{19}	1×10^{19}	8×10^{19}	8.47×10^{18}	1×10^{18}	2×10^{18}
Electron mobility μ_n ($cm^2\ V^{-1}\ s^{-1}$)	20	0.05	16	4500	90	0.2
Hole mobility μ_p ($cm^2\ V^{-1}\ s^{-1}$)	10	0.025	16	4500	90	0.2
Donor concentration N_D (cm^{-3})	2×10^{19}	1×10^{18}	0	1×10^{15}	0	0
Acceptor concentration NA (cm^{-3})	0	0	1×10^{15}	0	1×10^{15}	1×10^{18}
Defect density N_t (cm^{-3})	1×10^{15}	1×10^{15}	2.07×10^{14}	1×10^{15}	1×10^{15}	1×10^{15}

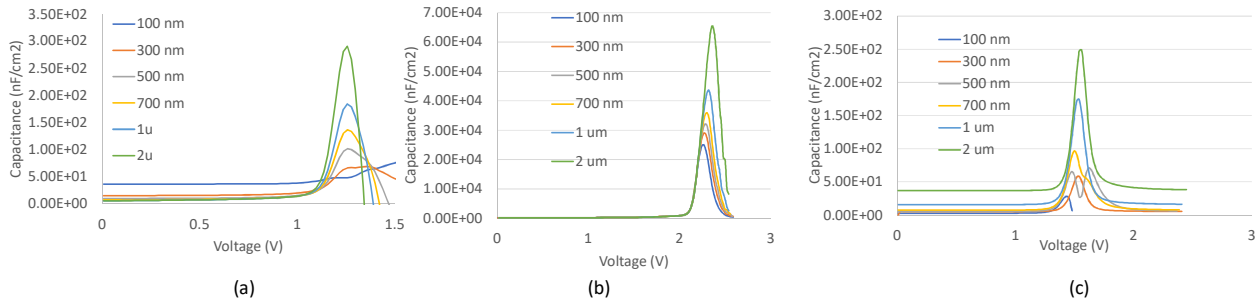

Figure 3. The C-V curve variation with respect to thickness of absorber layer of (a) $CsPbI_3$-based PSC, (b) $CsPbBr_3$-based PSC, and (c) $CsPbCl_3$-based PSC

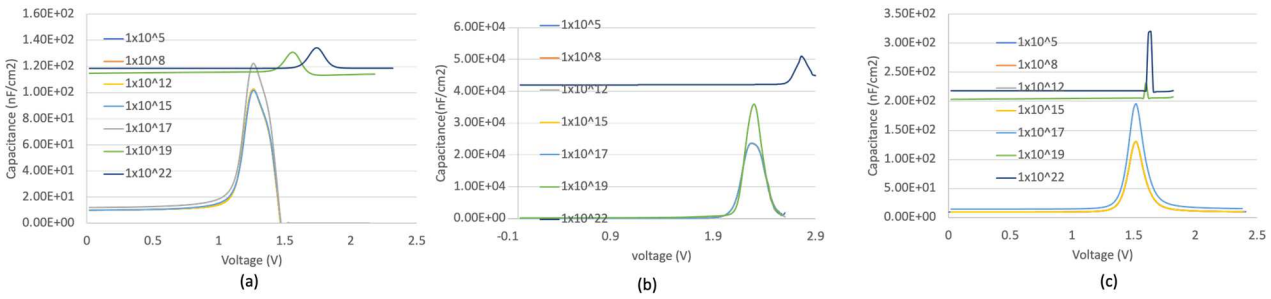

Figure 4. The C-V curve variation concerning the doping density of the absorber layer has been drawn as shown in curves (a) $CsPbI_3$, (b) $CsPbBr_3$, and (c) $CsPbCl_3$-based PSC.

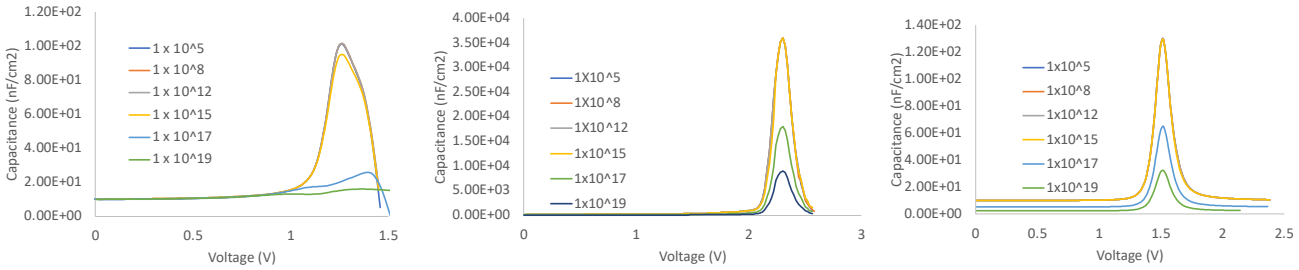

(a) (b) (c)

Figure 5. (a) C-V curve variation with respect to defect density of absorber layer of $CsPbI_3$-based PSC, (b) $CsPbBr_3$-based PSC, and (c) $CsPbCl_3$-based PSC

Clearly, the capacitance value remains the same as the defect density increases from $1x10^5$ cm^{-3} till it reaches its doping density as $1x10^{15}$ cm^{-3}, $1x10^{15}$ cm^{-3}, and $1x10^{15}$ cm^{-3} for $CsPbI_3$, $CsPbBr_3$, and $CsPbCl_3$-based PSC, respectively. Afterward, when the defect density exceeds the doping density, the capacitance value decreases as the absorber layer absorbs fewer photons and generates fewer electron-hole pairs. This will lead to fewer charges being accumulated at the interfaces. The C-V curve variation concerning the defect density of the absorber layer has been drawn as shown in curves (a) $CsPbI_3$, (b) $CsPbBr_3$, and (c) $CsPbCl_3$ in figure 5.

III. Conclusion

This study explores the effect of the performance of $CsPbX_3$-based PSCs. Simulations were processed using SCAPS, C-V curves, of three PSC structures with $CsPbI_3$, $CsPbBr_3$, and $CsPbCl_3$. The impact of three main simulation parameters on the C-V curves was deeply studied. The work demonstrated the capacitive behavior for the voltage, where various physical interpretations can be concluded.

Acknowledgment

The authors would like to acknowledge the support and contribution of the STDF in this work. As part of the STDF Project entitled, "Mesostructured Based Solar Cells for Smart Building Applications," Project ID#33502

References

[1] Q. Lu *et al.*, "A review on encapsulation technology from organic light emitting diodes to organic and perovskite solar cells," *Advanced Functional Materials,* vol. 31, no. 23, p. 2100151, 2021.

[2] A. M. Mahran and S. O. Abdellatif, "Optoelectronic Modelling and Analysis of Transparency against Efficiency in Perovskites/Dye-based Solar Cells," in *2021 International Conference on Microelectronics (ICM)*, 2021: IEEE, pp. 178-181.

[3] A. A. Eid, Z. S. Ismail, and S. O. Abdellatif, "Optimizing SCAPS model for perovskite solar cell equivalent circuit with utilizing Matlab-based parasitic resistance estimator algorithm," in *2020 2nd Novel Intelligent and Leading Emerging Sciences Conference (NILES)*, 24-26 Oct. 2020 2020, pp. 503-507, DOI: 10.1109/NILES50944.2020.9257929.

[4] W. Zhu *et al.*, "High-efficiency (> 14%) and air-stable carbon-based, all-inorganic CsPbI2Br perovskite solar cells through a top-seeded growth strategy," *ACS Energy Letters,* vol. 6, no. 4, pp. 1500-1510, 2021.

[5] Z. Rao, W. Liang, H. Huang, J. Ge, W. Wang, and S. Pan, "High sensitivity and rapid response ultraviolet photodetector of a tetragonal CsPbCl 3 perovskite single crystal," *Optical Materials Express,* vol. 10, no. 6, pp. 1374-1382, 2020.

[6] Y. An, C. Wang, G. Cao, and X. Li, "Heterojunction Perovskite Solar Cells: Opto-Electro-Thermal Physics, Modeling, and Experiment," *ACS nano,* vol. 14, no. 4, pp. 5017-5026, 2020.

[7] C. F. Wang *et al.*, "Centimeter‐Sized Single Crystals of Two‐Dimensional Hybrid Iodide Double Perovskite (4, 4‐Difluoropiperidinium) 4AgBiI8 for High‐Temperature Ferroelectricity and Efficient X‐Ray Detection," *Advanced Functional Materials,* vol. 31, no. 13, p. 2009457, 2021.

[8] P. Xu, "All-inorganic perovskite CsPbI2Br as a promising photovoltaic absorber: a first-principles study," *Journal of Chemical Sciences,* vol. 132, no. 1, pp. 1-8, 2020.

[9] G.-H. Kim and D. S. Kim, "Development of perovskite solar cells with> 25% conversion efficiency," *Joule,* vol. 5, no. 5, pp. 1033-1035, 2021.

[10] H. Wang, Z. Dong, H. Liu, W. Li, L. Zhu, and H. Chen, "Roles of organic molecules in inorganic CsPbX3 perovskite solar cells," *Advanced Energy Materials,* vol. 11, no. 1, p. 2002940, 2021.

[11] J. Chen and W. C. Choy, "Efficient and Stable All‐Inorganic Perovskite Solar Cells," *Solar RRL,* vol. 4, no. 11, p. 2000408, 2020.

[12] T. Ma, S. Wang, Y. Zhang, K. Zhang, and L. Yi, "The development of all-inorganic CsPbX3 perovskite solar cells," *Journal of Materials Science,* vol. 55, no. 2, pp. 464-479, 2020.

[13] Q. Chen, X. Yang, Y. Zhou, and B. Song, "Zwitterions: promising interfacial/doping materials for organic/perovskite solar cells," *New Journal of Chemistry,* vol. 45, no. 34, pp. 15118-15130, 2021.

[14] O. Al-Saban and S. O. Abdellatif, "Optoelectronic materials informatics: utilizing random-forest machine learning in optimizing the harvesting capabilities of mesostructured-based solar cells," in *2021 International Telecommunications Conference (ITC-Egypt)*, 2021: IEEE, pp. 1-4.

[15] M. M. Hassan, Z. S. Ismail, E. M. Hashem, R. Ghannam, and S. O. Abdellatif, "Investigating the tradeoff between transparency and efficiency in semitransparent bifacial mesosuperstructured solar cells for millimeter-scale applications," *IEEE Journal of photovoltaics,* vol. 11, no. 5, pp. 1222-1235, 2021.

[16] T. Hatem, Z. Ismail, M. G. Elmahgary, R. Ghannam, M. A. Ahmed, and S. O. Abdellatif, "Optimization of organic meso-superstructure solar cells for underwater IoT 2 self-powered sensors," *IEEE transactions on electron devices,* vol. 68, no. 10, pp. 5319-5321, 2021.